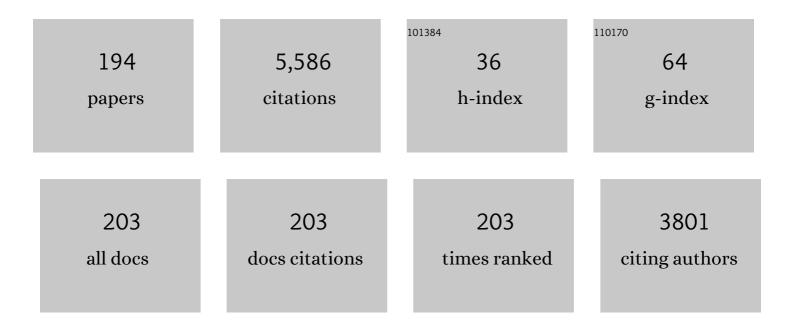
List of Publications by Year in descending order

Source: https://exaly.com/author-pdf/986671/publications.pdf Version: 2024-02-01



#	Article	IF	CITATIONS
1	Ultragrain refinement of plain low carbon steel by cold-rolling and annealing of martensite. Acta Materialia, 2002, 50, 4177-4189.	3.8	322
2	Novel Co-rich high performance twinning-induced plasticity (TWIP) and transformation-induced plasticity (TRIP) high-entropy alloys. Scripta Materialia, 2019, 165, 39-43.	2.6	200
3	Build direction dependence of microstructure and high-temperature tensile property of Co–Cr–Mo alloy fabricated by electron beam melting. Acta Materialia, 2014, 64, 154-168.	3.8	163
4	Relationship between the microstructure and mechanical properties of an equiatomic AlCoCrFeNi high-entropy alloy fabricated by selective electron beam melting. Materials Science & Engineering A: Structural Materials: Properties, Microstructure and Processing, 2016, 656, 39-46.	2.6	144
5	Strain-induced martensitic transformation near twin boundaries in a biomedical Co–Cr–Mo alloy with negative stacking fault energy. Acta Materialia, 2013, 61, 1648-1661.	3.8	140
6	Toughness of Ultrafine Grained Ferritic Steels Fabricated by ARB and Annealing Process. Materials Transactions, 2004, 45, 2272-2281.	0.4	139
7	Novel Co-rich high entropy alloys with superior tensile properties. Materials Research Letters, 2019, 7, 82-88.	4.1	139
8	First demonstration of promising selective electron beam melting method for utilizing high-entropy alloys as engineering materials. Materials Letters, 2015, 159, 12-15.	1.3	133
9	CoCrFeNiTi-based high-entropy alloy with superior tensile strength and corrosion resistance achieved by a combination of additive manufacturing using selective electron beam melting and solution treatment. Materials Letters, 2017, 189, 148-151.	1.3	130
10	Phase and grain size inhomogeneity and their influences on creep behavior of Co–Cr–Mo alloy additive manufactured by electron beam melting. Acta Materialia, 2015, 86, 305-318.	3.8	121
11	Formation of nanocrystalline surface layers in various metallic materials by near surface severe plastic deformation. Science and Technology of Advanced Materials, 2004, 5, 145-152.	2.8	105
12	Effect of rolling reduction on ultrafine grained structure and mechanical properties of low-carbon steel thermomechanically processed from martensite starting structure. Science and Technology of Advanced Materials, 2004, 5, 153-162.	2.8	100
13	In-situ fabrication and characterization of ultrafine structured Cu–TiC composites with high strength and high conductivity by mechanical milling. Journal of Alloys and Compounds, 2016, 657, 122-132.	2.8	95
14	Microstructural change of ultrafine-grained aluminum during high-speed plastic deformation. Materials Science & Engineering A: Structural Materials: Properties, Microstructure and Processing, 2003, 350, 108-116.	2.6	93
15	Hot forging characteristic of Ti–5Al–5V–5Mo–3Cr alloy with single metastable β microstructure. Materials Science & Engineering A: Structural Materials: Properties, Microstructure and Processing, 2014, 611, 337-344.	2.6	85
16	Impact of solute elements on detwinning in magnesium and its alloys. International Journal of Plasticity, 2017, 91, 134-159.	4.1	81
17	Enhanced damping capacity of magnesium alloys by tensile twin boundaries. Scripta Materialia, 2015, 101, 8-11.	2.6	80
18	Suzuki segregation in Co–Ni-based superalloy at 973 K: An experimental and computational study by phase-field simulation. Acta Materialia, 2012, 60, 2901-2915.	3.8	79

Үиісніко Коідимі

#	Article	IF	CITATIONS
19	Refinement of lamellar structures in Ti-Al alloy. Acta Materialia, 2017, 125, 81-97.	3.8	78
20	Effects of sigma phase and carbide on the wear behavior of CoCrMo alloys in Hanks' solution. Wear, 2014, 310, 51-62.	1.5	69
21	Mechanical and corrosion properties of AlCoCrFeNi high-entropy alloy fabricated with selective electron beam melting. Additive Manufacturing, 2018, 23, 264-271.	1.7	69
22	Molten pool behavior and effect of fluid flow on solidification conditions in selective electron beam melting (SEBM) of a biomedical Co-Cr-Mo alloy. Additive Manufacturing, 2019, 26, 202-214.	1.7	69
23	Microstructures and mechanical properties of bulk nanocrystalline Fe–Al–C alloys made by mechanically alloying with subsequent spark plasma sintering. Science and Technology of Advanced Materials, 2004, 5, 133-143.	2.8	66
24	Anodic oxide nanotube layers on Ti–Ta alloys: Substrate composition, microstructure and self-organization on two-size scales. Corrosion Science, 2009, 51, 1528-1533.	3.0	61
25	Cu–Ti–C alloy with high strength and high electrical conductivity prepared by two-step ball-milling processes. Materials & Design, 2014, 61, 70-74.	5.1	61
26	Electron beam additive manufacturing of Inconel 718 alloy rods: Impact of build direction on microstructure and high-temperature tensile properties. Additive Manufacturing, 2018, 23, 457-470.	1.7	60
27	Regulating twin boundary mobility by annealing in magnesium and its alloys. International Journal of Plasticity, 2017, 99, 1-18.	4.1	59
28	Local strain evolution due to athermal γ→ε martensitic transformation in biomedical Co Cr Mo alloys. Journal of the Mechanical Behavior of Biomedical Materials, 2014, 32, 52-61.	1.5	57
29	Mechanical and corrosion properties of CoCrFeNiTi-based high-entropy alloy additive manufactured using selective laser melting. Additive Manufacturing, 2019, 25, 412-420.	1.7	54
30	Regulating the coarsening of the $\hat{I}^3 \hat{e}^2$ phase in superalloys. NPG Asia Materials, 2015, 7, e212-e212.	3.8	52
31	Deformation Behavior and Dynamic Recrystallization of Biomedical Co-Cr-W-Ni (L-605) Alloy. Metallurgical and Materials Transactions A: Physical Metallurgy and Materials Science, 2013, 44, 2819-2830.	1.1	44
32	Porous metal produced by selective laser melting with effective isotropic thermal conductivity close to the Hashin–Shtrikman bound. International Journal of Heat and Mass Transfer, 2017, 105, 564-572.	2.5	43
33	Effects of partially substituting cobalt for nickel on the corrosion resistance of a Ni–16Cr–15Mo alloy to aqueous hydrofluoric acid. Corrosion Science, 2014, 78, 101-110.	3.0	40
34	Effects of alloyed Si on the oxidation behaviour of Co–29Cr–6Mo alloy for solid-oxide fuel cell interconnects. Corrosion Science, 2015, 95, 88-99.	3.0	40
35	Influence of cobalt addition on microstructure and hot workability of IN713C superalloy. Materials and Design, 2017, 122, 340-346.	3.3	40
36	Fatigue improvement of electron beam melting-fabricated biomedical Co–Cr–Mo alloy by accessible heat treatment. Materials Research Letters, 2018, 6, 93-99.	4.1	40

#	Article	IF	CITATIONS
37	Study of microstructure evolution and properties of Cu-Fe microcomposites produced by a pre-alloyed powder method. Materials and Design, 2017, 126, 64-72.	3.3	39
38	On microstructural homogenization and mechanical properties optimization of biomedical Co-Cr-Mo alloy additively manufactured by using electron beam melting. Additive Manufacturing, 2019, 28, 215-227.	1.7	38
39	Metallurgical aspects on the formation of self-organized anodic oxide nanotube layers. Electrochimica Acta, 2009, 54, 5155-5162.	2.6	37
40	Interfacial reactions of solid Co and solid Fe with liquid Al. Corrosion Science, 2012, 60, 32-37.	3.0	37
41	Role of nitrogen addition in stabilizing the γ phase of Biomedical Co–29Cr–6Mo alloy. Materials Chemistry and Physics, 2012, 133, 29-32.	2.0	37
42	High-stiffness and strength porous maraging steel via topology optimization and selective laser melting. Additive Manufacturing, 2017, 18, 194-202.	1.7	36
43	Role of strain-induced martensitic transformation on extrusion and intrusion formation during fatigue deformation of biomedical Co–Cr–Mo–N alloys. Acta Materialia, 2014, 81, 377-385.	3.8	35
44	Interfacial reactions between molten Al and a Co–Cr–Mo alloy with and without oxidation treatment. Corrosion Science, 2011, 53, 4324-4326.	3.0	34
45	Effects of cold working on corrosion resistance of Co-modified Ni–16Cr–15Mo alloy in hydrofluoric acid solution. Corrosion Science, 2014, 89, 258-267.	3.0	34
46	Dynamic recrystallization in biomedical Co-29Cr-6Mo-0.16N alloy with low stacking fault energy. Materials Science & Engineering A: Structural Materials: Properties, Microstructure and Processing, 2016, 668, 86-96.	2.6	34
47	Cellular lattices of biomedical Co-Cr-Mo-alloy fabricated by electron beam melting with the aid of shape optimization. Additive Manufacturing, 2016, 12, 305-313.	1.7	34
48	Characterisation of oxide films formed on Co–29Cr–6Mo alloy used in die-casting moulds for aluminium. Corrosion Science, 2013, 73, 72-79.	3.0	33
49	Osseointegration Enhancement by Zr doping of Co-Cr-Mo Implants Fabricated by Electron Beam Melting. Additive Manufacturing, 2015, 6, 6-15.	1.7	32
50	Heterogeneous microstructures and corrosion resistance of biomedical Co-Cr-Mo alloy fabricated by electron beam melting (EBM). Additive Manufacturing, 2018, 24, 103-114.	1.7	32
51	High damping capacity of ultra-fine grained aluminum produced by accumulative roll bonding. Journal of Alloys and Compounds, 2003, 355, 47-51.	2.8	31
52	Microscopic mechanism of plastic deformation in a polycrystalline Co–Cr–Mo alloy with a single hcp phase. Acta Materialia, 2014, 64, 1-11.	3.8	30
53	Elucidating the effect of preheating temperature on melt pool morphology variation in Inconel 718 laser powder bed fusion via simulation and experiment. Additive Manufacturing, 2021, 37, 101642.	1.7	30
54	Influence of Mo concentration on corrosion resistance to HF acid solution of Ni–Co–Cr–Mo alloys with and without Cu. Corrosion Science, 2015, 99, 185-193.	3.0	29

#	Article	IF	CITATIONS
55	Effect of process parameters on melt pool geometry and microstructure development for electron beam melting of IN718: A systematic single bead analysis study. Additive Manufacturing, 2019, 26, 215-226.	1.7	28
56	Corrosion resistance of Cu- and Fe-modified Ni–30Co–16Cr–15Mo alloy in aqueous hydrofluoric acid. Corrosion Science, 2014, 89, 81-92.	3.0	27
57	Regulating the passive film of NiCoCrMo alloy in hydrofluoric acid solution by small addition of Cu. Corrosion Science, 2015, 98, 119-127.	3.0	27
58	Isotropic Ti–6Al–4V lattice via topology optimization and electron-beam melting. Additive Manufacturing, 2018, 22, 634-642.	1.7	27
59	Thermal properties of powder beds in energy absorption and heat transfer during additive manufacturing with electron beam. Powder Technology, 2021, 381, 44-54.	2.1	27
60	Solute and vacancy segregation to a/4<1 1 1> and a/2<1 0 0> antiphase domain boundaries in Fe3Al. Acta Materialia, 2008, 56, 5861-5874.	3.8	26
61	Interfacial reaction between Co–Cr–Mo alloy and liquid Al. Corrosion Science, 2013, 75, 262-268.	3.0	26
62	Interdiffusion in Co Solid Solutions of Co-Al-Cr-Ni System at 1423 K. Materials Transactions, 2003, 44, 63-71.	0.4	25
63	Selective dissolution of nanolamellar Ti–41 at.% Al alloy single crystals. Acta Materialia, 2010, 58, 2876-2886.	3.8	25
64	Effects of plastic deformation on lamellar structure formation in Ti–39at.% Al single crystals. Acta Materialia, 2010, 58, 1104-1115.	3.8	25
65	Grain refinement due to complex twin formation in rapid hot forging of magnesium alloy. Scripta Materialia, 2013, 68, 171-174.	2.6	25
66	Submicron lamellar porous structure formed by selective dissolution of Ti-Al alloy. Materials and Design, 2016, 98, 1-11.	3.3	25
67	Tribological properties of carbon/carbon composites with various pyrolytic carbon microstructures. Wear, 2013, 304, 103-108.	1.5	24
68	Collective behavior of strain-induced martensitic transformation (SIMT) in biomedical Co–Cr–Mo–N alloy polycrystal: An ex-situ electron backscattering diffraction study. Materials Science & Engineering A: Structural Materials: Properties, Microstructure and Processing, 2014, 611, 263-273.	2.6	24
69	Precipitation behavior of a novel cobalt-based superalloy subjected to prior plastic deformations. Materials and Design, 2016, 112, 1-10.	3.3	24
70	Microstructural control of alloy 718 fabricated by electron beam melting with expanded processing window by adaptive offset method. Materials Science & Engineering A: Structural Materials: Properties, Microstructure and Processing, 2019, 764, 138058.	2.6	24
71	Pt diffusion in B2-type ordered NiAl intermetallic compound and its diffusion mechanisms. Science and Technology of Advanced Materials, 2000, 1, 237-249.	2.8	23
72	Influence of carbon and nitrogen addition on microstructure and hot deformation behavior of biomedical Co–Cr–Mo alloy. Materials Chemistry and Physics, 2012, 135, 849-854.	2.0	23

#	Article	IF	CITATIONS
73	Experimental and theoretical research on interfacial reaction of solid Co with liquid Al. Corrosion Science, 2013, 73, 54-61.	3.0	23
74	Modeling Grain Boundary Motion and Dynamic Recrystallization in Pure Metals. Metallurgical and Materials Transactions A: Physical Metallurgy and Materials Science, 2013, 44, 5861-5875.	1.1	23
75	Damping capacity of pre-compressed magnesium alloys after annealing. Materials Science & Engineering A: Structural Materials: Properties, Microstructure and Processing, 2017, 708, 104-109.	2.6	23
76	Comprehensive study on mechanisms for grain morphology evolution and texture development in powder bed fusion with electron beam of Co–Cr–Mo alloy. Materialia, 2019, 6, 100346.	1.3	23
77	Oxygen diffusion in Ti ₃ Al single crystals. Philosophical Magazine, 2008, 88, 2991-3010.	0.7	22
78	Development of low-Young's modulus Ti–Nb-based alloys with Cr addition. Journal of Materials Science, 2019, 54, 8675-8683.	1.7	22
79	Control of Crystallographic Texture and Mechanical Properties of Hastelloy-X via Laser Powder Bed Fusion. Crystals, 2021, 11, 1064.	1.0	22
80	Effects of carbon addition on wear mechanisms of CoCrMo metal-on-metal hip joint bearings. Materials Science and Engineering C, 2017, 76, 997-1004.	3.8	21
81	Discontinuous yielding and microstructural evolution of Ti-40Âat.% Al alloy compressed in single α-hcp phase region. Journal of Alloys and Compounds, 2017, 693, 1261-1276.	2.8	21
82	Electron beam melting of boron-modified Ti–6Al–2Sn–4Zr–2Mo–0.1Si alloy with superior tensile strength and oxidation resistance at elevated temperatures. Materialia, 2018, 4, 367-372.	1.3	21
83	Equiaxed grain formation by intrinsic heterogeneous nucleation via rapid heating and cooling in additive manufacturing of aluminum-silicon hypoeutectic alloy. Journal of Alloys and Compounds, 2022, 919, 165812.	2.8	21
84	Solid solubility of carbon in copper mechanically alloyed. Journal of Materials Science Letters, 2001, 20, 259-260.	0.5	20
85	Growth kinetics of antiphase domain in Ti3Al intermetallic compound. Science and Technology of Advanced Materials, 2004, 5, 19-28.	2.8	20
86	Effects of antiphase domains on dislocation motion in Ti ₃ Al single crystals deformed by prism slip. Philosophical Magazine, 2008, 88, 465-488.	0.7	20
87	Effect of nitriding treatment on corrosion behaviour of Co–Cr–Mo alloy in liquid Al. Corrosion Science, 2014, 78, 244-250.	3.0	20
88	Ex-situ observation on the dissolution behaviour of Ni–16Cr–15Mo and Ni–30Co–16Cr–15Mo alloys in hydrofluoric acid. Corrosion Science, 2015, 90, 133-139.	3.0	20
89	Strain-controlled iso-thermal fatigue behavior of Co–29Cr–6Mo used for tooling materials in Al die casting. Materials Science & Engineering A: Structural Materials: Properties, Microstructure and Processing, 2017, 703, 27-36.	2.6	20
90	Fundamentals of Metal 3D Printing Technologies. Materia Japan, 2017, 56, 686-690.	0.1	20

#	Article	IF	CITATIONS
91	Inverse Columnar-Equiaxed Transition (CET) in 304 and 316L Stainless Steels Melt by Electron Beam for Additive Manufacturing (AM). Crystals, 2021, 11, 856.	1.0	20
92	Effects of solute and vacancy segregation on migration of a/4ã€^111〉 and a/2ã€^100〉 antiphase bounda Fe3Al. Acta Materialia, 2009, 57, 3039-3051.	ries in 3.8	19
93	Detwining in Mg alloy with a high density of twin boundaries. Science and Technology of Advanced Materials, 2014, 15, 035003.	2.8	19
94	Effects of Al, Ti, and Zr doping on oxide film formation in Co–29Cr–6Mo alloy used as mould material for Al die-casting. Corrosion Science, 2014, 84, 147-158.	3.0	19
95	Characterization of powder bed generation in electron beam additive manufacturing by discrete element method (DEM). Materials Today: Proceedings, 2017, 4, 11437-11440.	0.9	19
96	Microstructure evolution of SUS303 free-cutting steel during hot compression process. Materials Science & Engineering A: Structural Materials: Properties, Microstructure and Processing, 2013, 583, 161-168.	2.6	18
97	Control of γ lamella precipitation in Ti–39 at.% Al single crystals by nanogroove-induced dislocation bands. Acta Materialia, 2015, 96, 352-365.	3.8	18
98	Effect of Building Position on Phase Distribution in Co-Cr-Mo Alloy Additive Manufactured by Electron-Beam Melting. Materials Transactions, 2016, 57, 2041-2047.	0.4	18
99	Energies of conservative and non-conservative antiphase boundaries in Ti3Al: a first principles study. Philosophical Magazine, 2006, 86, 1243-1259.	0.7	17
100	Superthermostability of nanoscale TIC-reinforced copper alloys manufactured by a two-step ball-milling process. Philosophical Magazine, 2015, 95, 4035-4053.	0.7	17
101	Investigation on hot deformation behavior of nanoscale TiC-strengthened Cu alloys fabricated by mechanical milling. Materials Science & Engineering A: Structural Materials: Properties, Microstructure and Processing, 2016, 668, 1-12.	2.6	17
102	Isothermal γ → Îμ phase transformation behavior in a Co-Cr-Mo alloy depending on thermal history during electron beam powder-bed additive manufacturing. Journal of Materials Science and Technology, 2020, 50, 162-170.	5.6	16
103	Plastic deformation behaviour and dislocation structure in Ti3Al single crystals cyclically deforming by prism slip. Acta Materialia, 1998, 46, 4311-4324.	3.8	15
104	Asymmetric slip trace formation in tension/compression cyclic deformation of biomedical Co–Cr–Mo–N alloy with negative stacking fault energy. Scripta Materialia, 2014, 74, 52-55.	2.6	15
105	Cr segregation at C11b/C40 interface in MoSi2-based alloys: A first-principles study. Intermetallics, 2013, 42, 165-169.	1.8	14
106	Uneven damage on head and liner contact surfaces of a retrieved Co–Cr-based metal-on-metal hip joint bearing: An important reason for the high failure rate. Materials Science and Engineering C, 2016, 62, 532-543.	3.8	14
107	Simulations of Non-Equilibrium and Equilibrium Segregation in Nickel-Based Superalloy Using Modified Scheil-Gulliver and Phase-Field Methods. Materials Transactions, 2020, 61, 2072-2078.	0.4	14
108	Nitriding of Co–Cr–Mo alloy in nitrogen. Materials Chemistry and Physics, 2014, 145, 350-356.	2.0	13

#	Article	IF	CITATIONS
109	Quantitative in vivo biocompatibility of new ultralowâ€nickel cobalt–chromium–molybdenum alloys. Journal of Orthopaedic Research, 2016, 34, 1505-1513.	1.2	13
110	Dynamic recrystallization behavior of biomedical Co-29Cr-6Mo-0.16N alloy. Materials Characterization, 2016, 118, 50-56.	1.9	13
111	Development of Novel Methods for Compensation of Stress-strain Curves. ISIJ International, 2011, 51, 782-787.	0.6	13
112	Mechanical Properties as a Function of Grain Size in Ultrafine Grained Aluminum and Iron Fabricated by ARB and Annealing Process. Materials Science Forum, 2003, 426-432, 2667-2672.	0.3	12
113	Effects of solute and vacancy segregation on antiphase boundary migration in stoichiometric and Al-rich Fe3Al: A phase-field simulation study. Intermetallics, 2010, 18, 1297-1302.	1.8	12
114	Mechanisms of Cr segregation to C11b/C40 lamellar interface in (Mo,Nb)Si2 duplex silicide: A phase-field study to bridge experimental and first-principles investigations. Intermetallics, 2014, 54, 232-241.	1.8	12
115	Significant impact of yttrium microaddition on high temperature tensile properties of Inconel 713C superalloy. Materials Letters, 2018, 227, 40-43.	1.3	12
116	Dislocation dipoles in cyclically deformed Ti3Al single crystals. Intermetallics, 2000, 8, 179-186.	1.8	11
117	Fabrication of Surface Nanocrystalline Aluminum Alloys. Materials Science Forum, 2003, 426-432, 2753-2758.	0.3	11
118	Densification and Structural Evolution in Spark Plasma Sintering Process of Mechanically Alloyed Nanocrystalline Fe-23Al-6C Powder. Materials Transactions, 2003, 44, 1604-1612.	0.4	11
119	Thermo-mechanical fatigue test of a wrought Co-based alloy as potential tooling material for die casting. Materials Science & Engineering A: Structural Materials: Properties, Microstructure and Processing, 2014, 615, 164-168.	2.6	11
120	Analysis of Run-in-Stage Wear Behavior and Contact Mechanics of Metal-on-Metal Hip Joint Bearings with Different Radial Clearances. Materials Transactions, 2015, 56, 826-834.	0.4	11
121	Evolution of antiphase domain (APD)/lamella mixed microstructure in Ti–39at%Al single crystals. Materials Science & Engineering A: Structural Materials: Properties, Microstructure and Processing, 2008, 478, 147-153.	2.6	10
122	Selective pore growth on lamellar Ti–41at.%Al alloy. Electrochemistry Communications, 2013, 26, 117-120.	2.3	10
123	Effects of surface friction treatment on the in vitro release of constituent metals from the biomedical Co–29Cr–6Mo–0.16N alloy. Materials Science and Engineering C, 2016, 64, 260-268.	3.8	10
124	Pattern formation mechanism of directionally-solidified MoSi2/Mo5Si3 eutectic by phase-field simulation. Intermetallics, 2020, 116, 106590.	1.8	10
125	Construction of Processing Map for Biomedical Co-29Cr-6Mo-0.23C-0.14N Alloy by Using Compression Tests. Materials Transactions, 2011, 52, 780-786.	0.4	9
126	Quantitative evaluation in hot workability of SUS303 free-cutting steel. Materials Science & Engineering A: Structural Materials: Properties, Microstructure and Processing, 2013, 563, 117-124.	2.6	9

#	Article	IF	CITATIONS
127	Effect of Phase Transformation on Tensile Behavior of Co–Cr–Mo Alloy Fabricated by Electron-beam Melting. Funtai Oyobi Fummatsu Yakin/Journal of the Japan Society of Powder and Powder Metallurgy, 2014, 61, 234-242.	0.1	9
128	Nano-lamellar/nano-tubular hierarchical porous structure produced by selective dissolution and anodization of lamellar Ti-40at.% Al alloy. Materials Letters, 2015, 145, 15-18.	1.3	9
129	Low Young's Modulus Ti–Nb–O with High Strength and Good Plasticity. Materials Transactions, 2018, 59, 858-860.	0.4	9
130	Nanoplastic deformation on Ti–39 at.% Al single crystals for manipulation of every single γ lamella. Acta Materialia, 2014, 76, 331-341.	3.8	8
131	The hot forging behaviour and its effects on the oxidation behaviour of W–Cr alloy. Corrosion Science, 2014, 83, 367-374.	3.0	8
132	Prototyping of Co–Cr–Mo Alloy Flat Spiral Spring by Electron Beam Melting. Funtai Oyobi Fummatsu Yakin/Journal of the Japan Society of Powder and Powder Metallurgy, 2014, 61, 243-249.	0.1	8
133	Mechanisms of lamellar structure formation and Cr interfacial segregation in C11b-MoSi2/C40-NbSi2 dual phase silicide verified by a phase-field simulation incorporating elastic inhomogeneity. Computational Materials Science, 2015, 108, 358-366.	1.4	8
134	Formation and stability of saturated bundled structure (SBS) in Ti3Al single crystals cyclically deformed by double prism slip. Acta Materialia, 1998, 46, 4743-4754.	3.8	7
135	Magneto-mechanical and Pseudoelastic Damping of Fe–Al Based Single Crystals. ISIJ International, 2009, 49, 1630-1635.	0.6	7
136	Effect of impurity atoms on α2/γ lamellar interfacial misfit in Ti–Al alloy: a systematic first principles study. Philosophical Magazine, 2011, 91, 3685-3704.	0.7	7
137	Dynamic Phase Transformation during Hot-Forging Process of a Powder Metallurgy α+β Titanium Alloy. Materials Transactions, 2012, 53, 1007-1010.	0.4	7
138	Enhanced Grain Refinement Through Deformation Induced α Precipitation in Hot Working of α + β Tita Alloy. Advanced Engineering Materials, 2012, 14, 785-789.	anium 1.6	7
139	Effect of Cobalt Addition on the Deformation and Recrystallization Textures of Polycrystalline IN713C Nickel Based Superalloy. Advanced Materials Research, 0, 922, 711-715.	0.3	7
140	Numerical study on the effective stiffness of topology-optimized lattice structures made of orthotropic crystal grains with optimal orientation. Computational Materials Science, 2019, 159, 202-209.	1.4	7
141	Precipitation during γ-ε Phase Transformation in Biomedical Co-Cr-Mo Alloys Fabricated by Electron Beam Melting. Metals, 2020, 10, 71.	1.0	7
142	Density, surface tension, and viscosity of Co-Cr-Mo melts measured using electrostatic levitation technique. Thermochimica Acta, 2022, 710, 179183.	1.2	7
143	Plastic deformation and fracture behaviour of Ti3Al single crystals deformed at high temperatures under cyclic loading. Acta Materialia, 1999, 47, 2019-2029.	3.8	6
144	Impact Consolidation of Mixed Copper and Carbon Powders Mechanically Alloyed Funtai Oyobi Fummatsu Yakin/Journal of the Japan Society of Powder and Powder Metallurgy, 2001, 48, 9-14.	0.1	6

#	Article	IF	CITATIONS
145	Anomalous growth of antiphase domains in Ti3Al. Scripta Materialia, 2009, 60, 144-147.	2.6	6
146	First-principles study on phase stability of MoSi <mml:math xmlns:mml="http://www.w3.org/1998/Math/MathML" display="inline"><mml:msub><mml:mrow /><mml:mn>2</mml:mn></mml:mrow </mml:msub>-NbSi<mml:math xmlns:mml="http://www.w3.org/1998/Math/MathML" display="inline"><mml:msub><mml:mrow /><mml:mn>2</mml:mn></mml:mrow </mml:msub>pseudobinary alloys. Physical Review B, 2012, 85, .</mml:math </mml:math 	1.1	6
147	Manipulating local heat accumulation towards controlled quality and microstructure of a Co-Cr-Mo alloy in powder bed fusion with electron beam. Materials Letters, 2019, 254, 269-272.	1.3	6
148	Modified Cellular Automaton Simulation of Metal Additive Manufacturing. Materials Transactions, 2021, 62, 864-870.	0.4	6
149	Optimization of Additive Manufacturing Process Utilizing Computer Simulation. Journal of Smart Processing, 2019, 8, 132-138.	0.0	6
150	Bulk Fe-Al-C Nanoalloys Made by Mechanically Alloying with Subsequent Spark Plasma Sintering and Their Mechanical Properties. Solid State Phenomena, 2005, 101-102, 103-110.	0.3	5
151	Phase-Field Simulation of <i>D</i> 0 ₃ -Type Antiphase Boundary Migration in Fe ₃ Al with Vacancy and Solute Segregation. Solid State Phenomena, 0, 172-174, 1313-1319.	0.3	5
152	Microstructures developed by super-rapid induction heating-and-quenching (SRIHQ) of Fe–1.4%Cr–1%C pearlitic steel. Materials Science & Engineering A: Structural Materials: Properties, Microstructure and Processing, 2013, 577, 29-35.	2.6	5
153	Porous surface structures in biomedical Co-Cr-Mo alloy prepared by local dealloying in a metallic melt. Materials Letters, 2018, 219, 256-259.	1.3	5
154	Low Springback and Low Young's Modulus in Ti–29Nb–13Ta–4.6Zr Alloy Modified by Mo Addition. Materials Transactions, 2019, 60, 1755-1762.	0.4	5
155	Manufacturing of a nanosized TiB strengthened Ti-based alloy via electron beam powder bed fusion. Additive Manufacturing, 2020, 36, 101472.	1.7	5
156	Co Diffusion in a B2-Type Ordered NiAl Compound. Nippon Kinzoku Gakkaishi/Journal of the Japan Institute of Metals, 2002, 66, 67-74.	0.2	5
157	Influence of CaO/SiO ₂ on the Reduction Behavior of Sintered Fe ₂ O ₃ –CaO–SiO ₂ –Al ₂ O ₃ Tablets at the Softening and Melting Temperatures. ISIJ International, 2020, 60, 1479-1486.	0.6	5
158	Thermophysical properties of liquid Co–Cr–Mo alloys measured by electromagnetic levitation in a static magnetic field. Thermochimica Acta, 2022, 708, 179119.	1.2	5
159	Effect of order-disorder transition on plastic anomaly of Ti3Al single crystals deforming by prism slip. Intermetallics, 1996, 4, 571-579.	1.8	4
160	Solid solubility of carbon in a mechanically alloyed Cu-29.7 At. Pct Zn alloy. Metallurgical and Materials Transactions A: Physical Metallurgy and Materials Science, 2001, 32, 1861-1862.	1.1	4
161	Internal Friction of Ultrafine-Grained Nickel Produced by Accumulative Roll-Bonding(ARB). Nippon Kinzoku Gakkaishi/Journal of the Japan Institute of Metals, 2005, 69, 997-1003.	0.2	4
162	Phase-Field Study on the Segregation Mechanism of Additive Elements in NbSi2/MoSi2 Duplex Silicide. Materials Research Society Symposia Proceedings, 2013, 1516, 145-150.	0.1	4

#	Article	IF	CITATIONS
163	Phase-Field Simulation of Lamellar Structure Formation in MoSi2/NbSi2 Duplex Silicide. Materials Research Society Symposia Proceedings, 2013, 1516, 309-315.	0.1	4
164	Effect of Building Position on Phase Distribution in Co-Cr-Mo Alloy Additive Manufactured by EBM. Funtai Oyobi Fummatsu Yakin/Journal of the Japan Society of Powder and Powder Metallurgy, 2016, 63, 10-16.	0.1	4
165	Coalescence Behavior of the Antiphase Domain in Ti ₃ Al. Defect and Diffusion Forum, 2001, 194-199, 577-582.	0.4	3
166	Impact and Static Consolidation of Mechanically-Alloyed Mixture of Copper and Graphite Powders. Radiation Effects and Defects in Solids, 2002, 157, 223-231.	0.4	3
167	Diffusion of Si in Ti ₃ Al Intermetallic Compound. Defect and Diffusion Forum, 2005, 237-240, 334-339.	0.4	3
168	Effects of substitutional impurity Au and Si atoms on antiphase boundary energies in Ti3Al: A first principles study. Philosophical Magazine, 2010, 90, 3919-3934.	0.7	3
169	Phase-Field Simulation of Antiphase Boundary Migration in Intermetallic Compounds with Solute and Vacancy Segregation. Materials Research Society Symposia Proceedings, 2011, 1295, 437.	0.1	3
170	Interface Migration with Segregation in MoSi ₂ -Based Lamellar Alloy Simulated by Phase-Field Method. Advanced Materials Research, 0, 922, 832-837.	0.3	3
171	Enhanced oxidation resistance of a titanium–based alloy by the addition of boron and the application of electron beam melting. Additive Manufacturing, 2020, 31, 100971.	1.7	3
172	Evaluation of Ordering Mobility from Antiphase Boundary Mobility in Fe3Al Using Phase-field Simulation. ISIJ International, 2012, 52, 1678-1682.	0.6	3
173	Current status of Metal Additive Manufacturing and Microstructure Control of Metal Parts in Powder Bed Fusionï¼^PBF). Journal of Smart Processing, 2018, 7, 216-222.	0.0	3
174	Spinodal Decomposition in Plastically Deformed Fe–Cr–Co Magnet Alloy. ISIJ International, 2022, 62, 1268-1274.	0.6	3
175	Additivity of Hardening by Nanolamellar Structure and Antiphase Domain in Ti-39at%Al Single Crystals. Materials Research Society Symposia Proceedings, 2008, 1086, 1.	0.1	2
176	Diffusion of Au in the Intermetallic Compound Ti3Al. Metallurgical and Materials Transactions A: Physical Metallurgy and Materials Science, 2009, 40, 2919-2926.	1.1	2
177	Phase-Field Simulation of Antiphase Boundary Migration in Slightly Off-stoichiometric Fe ₃ Al with Solute and Vacancy Segregation. Transactions of the Materials Research Society of Japan, 2010, 35, 209-215.	0.2	2
178	Introducing dislocations locally in Al-supersaturated α2-Ti3Al single crystal via nanoscale wedge indentation. Intermetallics, 2019, 113, 106557.	1.8	2
179	Melting and Solidification Behavior of 316L Steel Induced by Electron-Beam Irradiation for Additive Manufacturing. Journal of Smart Processing, 2021, 10, 208-213.	0.0	2
180	Comprehensive Phase Field Study on Directionally-Solidified MoSi ₂ /Mo ₅ Si ₃ Eutectic Alloy. Materials Science Forum, 0, 1016, 749-754.	0.3	2

#	Article	IF	CITATIONS
181	Diffusion Reactivity between Zinc Plate Layer and Nanocrystalline Surface Layer of IF Steel by Near Surface-Severe Plastic Deformation. Materials Science Forum, 2005, 502, 117-122.	0.3	1
182	Enhancement of Reaction of Zinc on Superficially Nanocrystallized IF Steel by Near Surface-Severe Plasitc Deformation. Materials Science Forum, 2006, 512, 361-366.	0.3	1
183	Dynamic Strain Aging in Biomedical Co–Cr–Mo-Based Alloys with Nitrogen Doping. Key Engineering Materials, 2012, 508, 141-145.	0.4	1
184	Dynamic Recrystallization of Biomedical Co-Cr-W-Ni (L-605) Alloy. Materials Science Forum, 0, 706-709, 472-477.	0.3	1
185	Reduction Behavior of Iron Oxide and Influence of Basicity in Initial Melt Formation Zone. Tetsu-To-Hagane/Journal of the Iron and Steel Institute of Japan, 2019, 105, 1099-1107.	0.1	1
186	Raking process for Powder Bed Fusion of Ti-6Al-4V alloy Powder Analyzed by Discrete Element Method. Keikinzoku/Journal of Japan Institute of Light Metals, 2022, 72, 291-297.	0.1	1
187	Reaction of Sn to Nanocrystalline Surface Layer of Cu by Near Surface Severe Plastic Deformation. Solid State Phenomena, 2007, 127, 115-120.	0.3	0
188	Phase-Field Study of Ordered Domain Growth and Segregation in Intermetallics. Materia Japan, 2012, 51, 53-61.	0.1	0
189	ãf•ã,§ãf¼ã,ºãf•ã,£ãf¼ãf«ãf‰æ³•ã«ã,^ã,< Ni 基è¶å•金ä»~åŠè£½é€ã«ãŠã⁵ã,‹å‡å›ºåæžëº^æ,¬. Journal of Smart	: Rocc essin	1002021, 1
190	Spinodal Decomposition in Plastically Deformed Fe-Cr-Co Magnet Alloy. Tetsu-To-Hagane/Journal of the Iron and Steel Institute of Japan, 2021, 107, 146-153.	0.1	0
191	Modified Cellular Automaton Simulation of Metal Additive Manufacturing. Nippon Kinzoku Gakkaishi/Journal of the Japan Institute of Metals, 2021, 85, 103-109.	0.2	0
192	Guide to Development of Innovative Joining Technology. Yosetsu Gakkai Shi/Journal of the Japan Welding Society, 2017, 86, 570-578.	0.0	0
193	Solidification and Process Optimization in Metal Additive Manufacturing. Journal of Japan Institute of Electronics Packaging, 2020, 23, 446-451.	0.0	0

194 金属ç©å±**ĕ**ی½¢ã«ãŠã'ã,‹ãf‡ã,ã,¿ãf«ãf,,ã,Ħf³æ§‹ç⁻‰ã®ãŸã,ã®è∽ç®—ç§'å¦ãëāf‡ãf¼ã,¿ç§'å¦. Journal of Smart **ðro**cessing 2021, 10